Liquid Crystal Variable Retarders for aerospace polarimetry applications

R. L. Heredero[a], N. Uribe-Patarroyo[a], T. Belenguer[a] G. Ramos[a]

A. Sánchez [a], M. Reina[a], V. Martínez Pillet[b], A. Álvarez-Herrero[a]

[a] Laboratorio de Instrumentación Espacial (LINES) [b] Laboratorio TERMICOS– Área de Cargas Útiles e Instrumentación – Instituto Nacional de Técnica Aerospacial (INTA) – Ctra. Ajalvir km 4 – 28850 Torrejón de Ardoz (Madrid) SPAIN

[b] Instituto de Astrofísica de Canarias (IAC), La Laguna - Tenerife - SPAIN

This paper presents the optical effects of different tests that simulate the aerospace environment on the Liquid Crystal Variable Retarders (LCVRs) used in the Imaging Magnetograph eXperiment (IMaX), postfocal instrument of the SUNRISE payload within the NASA Long Duration Balloon program. Analysis of the influence of vacuum, temperature, vibration, gamma and ultraviolet radiation is performed by measuring the effects of these tests on the optical retardance, the response time, the wavefront distortion and the transmittance, including some "in-situ" measurements. Outgassing measurements of the different parts of the LCVRs are also shown. From the results obtained it can be concluded that these optical devices are suitable and seem to be excellent candidates for aerospace platforms.

Copyright

OCIS codes: 160.3710 Liquid Crystals, 230.3720 Liquid-crystal devices, 260.5430 Polarization, 350.4800 Optical standards and testing, 160.4760 Optical properties, 120.6810 Thermal effects

Introduction

Liquid Crystal Variable Retarders (LCVRs) have been widely used as polarization devices for polarimetric applications providing a variable optical retardance without the need of moving any mechanical parts[1-5]. In this sense, they have been used in ground telescopes[6-8] and furthermore, they have a promising future in aerospace applications for polarization analysis thanks to their other advantages as low mass and low power consumption.

The Imaging Magnetograph eXperiment (IMaX)[9] is one of the three instruments of the payload of the SUNRISE balloon project within the NASA Long Duration Balloon program. SUNRISE is a stratospheric balloon to be flown from Antarctica to study solar magnetic fields resolving the critical length scale of 100 km in the solar photosphere.

IMaX is a diffraction limited imager which will carry out spectroscopic measurements with resolutions in the 50.000-100.000 range and capable to perform polarization measurements. Following this goal, IMaX works as a polarimeter (IMaX must be able to measure the four Stokes parameters of a Zeeman sensitive solar spectral line), as a spectrometer (IMaX should provide a spectral resolution better than 100 mÅ) and as a diffraction limited imager (IMaX must be diffraction limited, Strehl ratio > 0.8).

The solutions adopted by the project to fulfill all these goals have been the use of LCVR for the polarization modulation, one $LiNbO_3$ etalon in double pass provided by ACPO/CSIRO (Australian Center for Precision Optics) and two modern CCD detectors provided by Photonic

Science (custom made, based on the E2V CCD47-20 chip) that allow the application of phase diversity techniques[10] by slightly changing the focus of one of the CCDs.

Any on-board element used for aerospace applications must be space-qualified, i.e. it must be able to survive the hazards of operation in space due to harsh environmental conditions, and it must be low risk. The aim of this paper is to present the evaluation of the LCVRs performances for their use in IMaX-SUNRISE by following a campaign of tests to simulate the mission environmental conditions (Polar flight at 40 Km altitude). However, standard space environmental conditions have been considered in some cases to advance results for possible future aerospace developments. The experience that our consortium has acquired in the development of the IMaX magnetograph based on LCVRs will place the IMaX consortium in the vanguard of the aerospace applications with LCVRs, and will enable us to lead future developments as the Visible-Light Imaging Magnetograph (VIM) on board of ESA Solar Orbiter mission.

Results of optical retardance and response time as a function of applied voltage, which establish the features and reliability of LCVRs, are shown. Values of transmittance and wavefront distortion, which are important concerning the optical design of one instrument that includes LCVRs as active components, are also included in this paper.

Few previous works present only the LCVR survivability under extreme vacuum, temperature and radiation conditions[11] including measurements of optical retardance after exposure to gamma radiation[12]. Our paper presents measurements of the optical parameters mentioned above during thermal-vacuum cycling, and the change of the same parameters after vibration, landing shock, gamma and UV radiation tests. Outgassing measurements of the different materials than constitute the LCVR are also reported.

LCVR description

A LCVR consists of a nematic LC layer embedded between two glass (fused silica) plates, two transparent ITO (Indium Tin Oxide) conductive films and two alignment (polyimide) layers. The polyimide layer forces an initial orientation of the LC molecules in a direction parallel to that of the silica plates. By the application of a voltage through the ITO films, a homogenous electric field is generated inside the cavity that forces a reorientation of the LC molecules, thanks to the dielectric anisotropy they present. A balance between the anchoring forces due to the polyimide and the electric field must be reached, and that permits a variable final orientation of the molecules depending on the strength of the field. However, there exists a voltage, below of which no reorientation by the external field is possible. It is known as the threshold voltage, and defines the point at which the molecules begin to reorient, known as the Fréedericksz transition. This threshold voltage depends on the anchoring force and is linear with the square root of the splay elastic constant of the LC[13].

The detailed structure of the LCVRs to be used in IMaX is shown in Fig. 1. The substrate is fused silica polished to high optical quality (~λ/10 rms). The inner surface of the substrate is coated with a conductive ITO film, 250 Å thick (resistance < 200 Ω). Over the ITO layer, the uniform polyimide thin layer (200-300 nm) is deposited. The spacers define the thickness of the LC layer which will be inserted into the silica plates subsequently. The spacer used is a non-reactive plastic (Mylar), 6.5 μm thick. The cell is assembled and tacked together with a 90-minutes epoxy cured at 150 ºC (Struct Bond XN-5A). Then, it is filled with the LC and sealed with a slow curing epoxy (ThreeBond 3026 B, UV 300-400nm 10kJ/m^2). Finally, two external cables for voltage feeding are welded to the ITO layers with the epoxy ThreeBond 5030.

Two types of LCVRs have been selected for this test campaign: LCVR-type V: LC MLC-6204-100, $\Delta n = 0.1479$ at 525 nm and viscosity = 38 mm^2/s (@ 20 ºC) and LCVRs-type N: LC ZLI-2116-100, $\Delta n = 0.1226$ at 525 nm and viscosity = 19 mm^2/s (@ 20 ºC).

Test Campaign Description

Table 1 shows the tests that have been carried out in order to analyze the variation of the LCVR performances when they are immersed in a space environment.

All the optical parameters were measured before the start of each test in order to have a reference measurement. It is important to note that during the thermal-vacuum test, the optical parameters were measured *in situ* for different temperatures. In the rest of the tests, the optical parameters of interest were measured after the test to evaluate the changes.

Measurement of optical parameters

The voltage signals applied to the LCVR are square AC waves with a fixed frequency of 2 kHz with a DC compensation below 4 mV in the range of [0,14] peak volts, V_p. The voltage source was developed by the Instituto Astrofísico de Andalucía (IAA).

Retardance and response time measurements

The null ellipsometer used to measure the optical retardance (δ) and the response time (τ) of the LCVRs is an optical instrument usually employed to measure the optical properties of materials. It is based on the measurement of changes in the state of polarization and therefore it avoids intensity measurements by setting a minimum ("null" condition) of light power in the detector and provides directly the retardance value.

The ellipsometer configuration used was a PSCA (Polarizer-Sample-Compensator-Analyzer)[14] in transmission mode with a HeNe laser. Measurements following increase and decrease of the applied voltages were performed in order to identify possible hysteresis behavior.

The response time is the time needed for the LCVR to reach a new polarization state motivated by a voltage change. The state changes will be defined by two voltages (V_i, V_d) being V_i the voltage corresponding to the initial state and V_d the difference between the final (V_f) and initial states $V_d = V_f - V_i$. For the experimental acquisition, τ was defined as the time needed to change between 10% and 90% of the total intensity measured by the ellipsometer photodetector.

The retardance and response time measurements at different temperatures were performed with the two arms of the null ellipsometer located outside the thermal vacuum chamber (TVC) and placed onto two stabilized tables (similar to the setup shown in Fig. 2).

Wavefront error

In order to analyze the optical quality, the wavefront distortion when a beam is transmitted through the LCVR has been measured with a Fizeau interferometer (ZYGO GPI-XP) based on phase-modulated measurements. This is an important factor to be taken into account when designing an instrument.

The wavefront measurements at different temperatures were performed with the ZYGO interferometer placed outside the TVC and onto a stabilized table, and the LCVR under test mounted inside the TVC in the same mount used in the retardance measurements (see Fig. 2). The mount has two physical holes in order to be able to take one reference measurement as well as the LCVR measurement for each ambient condition. The interferometer beam goes through both, the LCVR and the reference plate holes; the beam is then folded by one mirror at 45º and goes down to one reference plate used to form the null cavity. The reference plate is a plane

parallel glass with an optical quality of ~λ/90 (where λ is the wavelength of the HeNe laser of the interferometer, 633 nm).

Transmittance

The measurements were carried out with an Optical Spectrum Analyzer (SPECTRO 320, Instrument Systems) from 350 to 800 nm always before and after the tests.

Results

Thermal-vacuum test

Before initializing the thermal-vacuum test, it was verified that the quartz windows of the TVC have no influence on the retardance measurements.

When the TVC was pumped down to ~ 10^{-5} mbar, the retardance showed no change under vacuum conditions.

The retardance measurements in vacuum made at different temperatures between −20 and +40 ºC are shown in Fig. 3. In this case all the measurements correspond to the rising of voltages.

Note that there are two measurements at +20 ºC: the first one was performed before the start of the test and the other one was performed when the LCVR had undergone seven complete temperature cycles. It is important to note that there was not appreciable hysteresis at none of the temperatures analyzed. From Fig. 3 it can be concluded that the LCVR retardance did not change after seven temperature cycles and this confirmed that the life time period of the LCVRs can operate within this temperature range (albeit with a different calibration).

From the data depicted in Fig. 3, it can be appreciated that the retardance changes more strongly with temperature for small voltages. If this was due to an effect of a change of refractive index of the molecules of the LC with temperature, the effect would be a constant factor equal for all voltages. Instead, the observed behavior is explained by the relation of the ordering of the LC molecules with temperature. The order parameter *S* is defined as (see Ref. 13):

$$S = \left\langle \frac{3}{2}\cos^2\theta - \frac{1}{2} \right\rangle \tag{1}$$

where θ stands for the angle between the main axis of a particular molecule and the average orientation of all molecules, and < > means an average over the entire system.

Defined in this way, S=1 corresponds to a perfectly aligned LC, and S=0 to an isotropic state. It is well known that S decreases with temperature[15] and that, near the nematic-isotropic transition temperature (T_c), it drops non-continuously to zero. The behavior with temperature can be explained because, as molecules gain energy, they can depart more from order than at lower temperatures, due to combined effects of entropy and energy. In the absence of applied voltage, the maximum retardance is obtained because the director is parallel to the interfaces. If not all the molecules are perfectly aligned in this direction (S<1), then the retardance is lower. Therefore, as temperature increases, S and δ decrease. Thus, from the measurements of retardance as a function of temperature, the behavior of S with temperature can be extracted.

Traditionally, retardance has been related to S through Haller's approximation[16,17], which involves a three parameter fitting procedure. However, the appropriateness of the Haller's approximation has been discussed recently[18] because it usually yields values of S which are not compatible with the ones predicted by theory[13]. The improved relationship derived in Ref. 18 augments the number of free parameters to fit, but our experimental data volume was found to be inappropriate for the use of this procedure. Because our intention is to estimate the order

parameter in our samples, an approximate calculation of S through the Haller's approximation will be used to be able to predict the general behavior in a wider range of temperatures:

$$\delta = \delta_0 \cdot S = \delta_0 \left(1 - \frac{T}{T_c}\right)^{\beta} \tag{2}$$

where δ_0 is the retardance for S=1 and β is a critical exponent related to the phase transition.

In Fig. 4 the fits of Eq. (2) to the experimental data are depicted, one in which all parameters are free (fit A), and the other one in which T_c was fixed with the known value of T_c = 66º C (information provided by supplier) for this particular LC (fit B). Fit A yields β = 0.156 ± 0.003 which is normal for the Haller's approximation, although it is not compatible with the theoretically predicted value of 0.25[13]. However, it is easy to see that a much better fit is obtained for case B, but values smaller than expected for both β and T_c are obtained. δ_0 value from fit B (535 ± 8) was used to normalize δ vs. T to obtain the order parameter, which is shown in the inset of Fig. 4. It can be appreciated from these approximations and the general behaviour of S that the sensitivity of the optical retardance with temperature decreases when the working temperatures are far from T_c.

When a voltage is applied, the behavior is more complex, as now the order parameter is affected by the strength of the applied field. Nevertheless, it is normal to assume that the higher the voltage, the lower the sensitivity of retardance with temperature, as the main role for the ordering of the molecules is assumed by the electric field. This effect can be visualized in Fig. 5 where the retardance measurements versus temperature for V_p = 0, 4, 8 and 14 V are shown with the same vertical scale for the last 3 measurements in order to better visualize the differences.

The response time measurements for different situations as a function of temperature from T= −13 ºC to +20 ºC are plotted in Fig. 6. The following different transition voltages were chosen because they correspond to standard retardance changes at RT: Case 1 (V_i = 6.50 V,V_d = −1.75 V) 90º to 135º, Case 2 (V_i = 4.00 V,V_d = −1.02 V) 180º to 270º, Case 3: (V_i = 4.00 V,V_d = 10.00 V) 180º to 0º and Case 4 (V_i = 6.50 V, V_d = 7.50 V) 90º to 0º.

It can be seen that the dependence of response time on temperature is simple for all voltage changes: as the temperature decreases, the response times increases, as expected due to the approach to the liquid-crystal to solid transition.

It is considered that the visco-elastic coefficient, γ_1/κ_1 (being γ_1 the rotational viscosity and κ_1 the splay elastic constant) plays the major role in response time temperature dependence (see Ref. 16) and found to be proportional to it[19]. As $\kappa_1 \propto S^2$, and $\gamma_1 \propto S^2 \cdot \mathrm{Exp}\{E/[k(T-T_0)]\}$ (see Ref. 16), where E is the diffusion activation energy and k Boltzmann's constant), it is obtained:

$$\tau = A \cdot e^{\frac{B}{k(T-T_0)}} \tag{3}$$

where A is a constant dependent on the particular transition, and B is a constant common for all transitions and dependent only on the LC.

In Fig. 6, the lines represent the simultaneous fit of all the experimental data to Eq. (3). It was found that Eq. (3) explains very well the observed behavior, and from all measurements T_0 = −65 ± 6 ºC and B/k=(3.1 ± 0.6)·10 K.

It can be concluded that depending on the application, the operating temperature could be chosen taking into account the information depicted in Fig 4 and the response time behavior since as temperature increases, response times are lower but maximum retardance for V_p = 0 V decreases.

In addition, it can be noted that the maximum response time takes place for the transition (4.00 V, −1.02 V), which corresponds to a change in retardance from 180 to 270 deg at RT. In this case the response time goes from 55 ms at RT up to 530 ms at −20ºC. As it is expected, the slower transitions are for negative values of V_d, and within them, the slowest one corresponds to a final state near the Freèdericksz transition. Meanwhile, the two transitions with positive V_d have very similar response times.

The rms value of the wavefront error measured for one LCVR-N was ~ λ/36.6 (λ= 633 nm) under vacuum conditions and with the TVC open and closed. That confirmed that there was no influence of the TVC windows.

Fig. 7 shows the rms values in nm measured for different temperatures when no voltage was applied. It is important to note that the null cavity wavefront error was much smaller than the changes observed in LCVR wavefront error during the thermal-vacuum test. From this plot it can be observed that in most of the situations, the quality of the LCVR increases as the temperature rises.

It was observed that the optical quality of the LCVR decreased after having suffered one thermal-vacuum cycle between −20 and +40 ºC. Before starting the test, the wavefront error was ~λ/35.71. This value increased to λ/30.3 when the vacuum went back to normal conditions and with the TVC closed and λ/27.8 when the TVC was opened.

The transmittance of the two LCVRs used for the retardance and response time measurements (seven thermal cycles between −35 and 40 ºC) and the wavefront error measurements (one cycle between −20 and 40 ºC) were measured after the thermal-vacuum tests described above. Fig. 8 shows the transmittance measured before, after the complete thermal-

vacuum tests and 2 months afterwards in the case of the LCVR used for retardance measurements, Fig. 8a.

The ITO coatings used to make the LCVR cavity also give rise to a low-finesse etalon whose intensity modulations can be observed in the wavelength transmission curves. As it can be seen in Fig. 8a and Fig. 8b, the changes after the thermal cycling and after 2 months stay within the amplitude of the etalon induced fluctuations.

Gamma radiation test

A ^{60}Co source was used inside a water pool at atmospheric pressure and room temperature. The sample holder was located inside the underwater casing at the adequate distance to irradiate with a dose rate of 500 rad/h. The ^{60}Co sources should be arranged inside the pool so that the dose received by the LCVR is homogeneous within ~ 90%.

The LCVR-V was irradiated up to 54 krad following three exposures at a dose rate of 500 rad/hour in order to study the response of the LCVRs to different total doses.

The LCVR optical parameters of interest were measured after ~12 h and during a two-month period after each step of γ dose in order to analyze its degradation and to study possible relaxation effects.

Fig. 9 shows the optical retardance measured after the LCVR has been irradiated with 10, 20 and 54 krad. It can be observed that the retardance does not change after 10 krad of γ-radiation and increases ~ 19 % after 20 krad and ~ 33 % after 54 krad for the voltage range (between 1 and 3 V) where there is a larger slope between voltage and retardance. There are not appreciable retardance variations for voltages before the Fréedericksz transition or when $V_p > 8$ V, i.e, retardance < 35 deg.

The response times measured after each irradiation step were performed between the same optical retardances and therefore, the voltages applied to the LCVRs were different in each case. The results measurements show that the response time measured after the LCVR was irradiated with doses of 10 and 20 krad increased; it can be also appreciated a diminution tendency in response time after a total dose of 54 krad possibly due to the different voltages applied in each case.

There are no clear differences between the wavefront deformation values measured before and after irradiations of 10 and 20 krad. After higher doses (54 krad), it could be appreciated a small diminution tendency in wavefront error.

The transmittance of the LCVR measured after having been irradiated is shown in Fig. 10. It can be clearly noted that the transmittance decreases with the total dose and this dependency is nearly linear for λ_{IMaX} = 525 nm (see inset of Fig. 10).

The reduction in the LCVR transmittance can be related to transmittance losses of the fused silica, the polyimide, the ITO conductive thin film and/or the LC. Since the ITO layer is very thin (250 Å thick), its influence can be discarded. On the other hand, it has been measured that the transmittance change of the fused silica after having received a total dose of 200 krad is negligible[15] compared to the transmittance changes shown in Fig. 10. Therefore, the drop of the transmittance of the LCVR can be mainly attributed to an effect on the polyimide or on the LC. Further studies will help to clarify this issue.

Some more measurements were performed during a two-month period in order to study possible relaxation processes of the molecules of the polyimide and/or the LC of the LCVR. It was observed that the transmittance stays at the same level two months and six months after having been irradiated with a total dose of 54 krad.

UV radiation Test

Previous space environment tests of LCs[11,12] show that the only damage occurs with UV exposure[11]. Since during SUNRISE flight the UV radiation received by the instruments will be negligible, the total doses considered in this test have been chosen according to previous studies in order to evaluate the use of the LCVR in future aerospace applications[11,12].

The test was performed at 25 ºC and a pressure between 1 and $5 \cdot 10^{-5}$ bar. The temperature of the LCVR during the test could not be controlled and some thermocouples placed onto the face looking at the UV source measured temperatures much higher than 25 ºC (~ 180 ºC in some cases), confirming that there is an enormous gradient of temperature between the surface of the holder and the surface of the LCVR which is facing the UV source.

It was observed by visual inspection that the LCVR turned yellowish after the first UV radiation exposure of ~ 30 ESH, and there was no retardance with or without applying voltages after this exposure. Therefore, it was observed that the LC is totally degraded under exposures of UV equals to ~ 30 ESH and some shielding would be needed when using these devices as polarization elements in an aerospace platform. However, the enormous gradient of temperature could have been the reason of degradation of the LCVR and further studies would have to be performed.

The wavefront error transmitted by two LCVRs was measured after each UV exposure. The rms value increased from $\lambda/28.57$ to $\lambda/8$ after an UV irradiation of ~ 61.41 ESH and in the other case, it increased from $\lambda/19.61$ to $\lambda/7.3$ after an UV irradiation of ~ 30.63 ESH. Thus UV radiation of tens of ESH not only prevents the proper functioning of the LCVR as a retarder, but it also increases the degradation of the transmitted wavefront error by the device.

Fig. 11 shows the transmittance of two different LCVRs from 350 to 800 nm after each step of UV exposure. It can be appreciated that the transmittance has decreased after the UV radiation.

The decrease in the LCVR transmittance can come from transmittance losses of the fused silica, the polyimide, the ITO conductive thin film and/or the LC. According to some previous studies found in the literature[20], the UV irradiation decreases significantly the transmittance of fused silica only between 200-400 nm and therefore, this effect will not affect the IMaX working wavelength. In order to study the effects of the rest of the LCVR components, two different fused silica samples were tested: one only with ITO and the other one with only polyimide; a third sample with fused silica, ITO and polyimide and without LC (sample called from now on "empty LCVR") was also submitted to the UV test. From the transmittance data obtained, it can be concluded that the transmittance of all the materials that constitute the LCVR decrease and follow the same behaviour with UV irradiation. However, the influence of the LC is determinant according to the measurements of the "empty LCVR". In order to evaluate each of them separately, data about transmission of fused silica after UV exposures would be needed.

Vibration and dynamic test

The LCVR to be tested was placed in the IMaX structural mount, which will hold two LCVRs and one pre-filter during SUNRISE mission. Different loads (random and shock) were applied on each axis in order to qualify the LCVR as well as the mechanical mount.

The retardance measured before and one week after vibration test shows an increment in the region of greatest slope. However, the retardance remains almost the same after the test for $V_p > 10$ V. Further studies need to be done to study the vibration effect.

The response times measured after the vibration test are within the limits of good performance for IMaX (a few ms).

It was observed that the wavefront deformation has a small tendency to increase after the vibration test.

It was observed a slight increment of the transmittance of ~ 3 % after the vibration test for λ_{IMaX} but it is important to note that the visibility of the Fabry-Perot interference decreased

Non-Operative Temperatures Test

According to standard procedures followed in Space Programs, after the vibration/dynamic test mentioned before, the LCVR was submitted to a thermal-vacuum test; the temperatures considered in this test were chosen according to the temperatures defined by the project in the non-operative limits: from −65 ºC to 70 ºC.

The LCVR was degraded after the test since the optical retardance did not change by applying different peak voltages and was always ~ 460 deg. The LC molecules normally support this range of temperatures and therefore, it can be concluded from this result that, even if the LC was still inside the fused silica cell, its operation performance was not adequate and further studies to asses the combined effect between vibration and non-operative temperatures are needed.

Outgassing Test

The vacuum chamber facility used for this test only accepted samples with dimensions ~ 2 × 2 cm^2 and therefore, only the elements more prone to outgassing under vacuum conditions have been individually analyzed: Struct Bond XN-5A (used to assemble the LCVR cell), ThreeBond

3026 B (used to seal the LCVR cell), ThreeBond 5030 (used to stick the cables on the LCVR fused silica) and the cables. The values obtained from the test are shown in Table 2.

The European Cooperation for Space Standardization[21] accepts WLT < 1% for outgassing of materials. If WLT > 1% and the WLR < 1%, the material is also acceptable. However, if WLT > 1% and the WLR > 1%, the component is not acceptable. For the volatiles mass, the standard accepts values of VCM < 0.1 %.

It can be seen from the values in Table 2 that none of the components of the LCVR used up to now fulfill the ESA standard recommendations but they are acceptable for the SUNRISE program since it is a short time mission. For future aerospace missions it would be necessary to define the outgassing limits and change the materials accordingly.

Acknowledgments

The authors wish to thank the Plan Nacional del Espacio (PNE) for financial support and TECDIS for the fabrication of the LCVRs. They are also very grateful with the Instituto Astrofísico de Andalucía for the support with the electronics to control the voltage applied to the LCVRs.

Conclusions

It can be concluded that these optical devices have a promising future for aerospace applications if some care is taken into account concerning the control of temperature and some shielding to avoid radiation but these are usual tasks in aerospace projects.

References

1. T. F. Drouillard II, P. A. Searcy, S. R. Davis, R. J. Uberna, R. A. Herke, M. H. Anderson, S. D. Rommel, E. B. Anthony, V. B. Damiao, "Polarimetry using Liquid Crystal Variable Retarders", in *Emerging Optoelectronic Applications*, E.G. Jabbour, J. T. Rantala eds., Proc. of the SPIE, **5363**, 86-97 (2004)
2. E. Garcia-Caurel, A. De Martino, B. Drévillon, "Spectroscopic Mueller polarimeter based on Liquid Crystal devices", Thin Solid Films **455** 120–123 (2004)
3. B. Laude-Boulesteix, A. De Martino, B. Drévillon, L. Schwartz, "Mueller polarimetric imaging system with Liquid Crystals", Appl. Optics **43**, 2824-2832 (2004)
4. J. M. Bueno, "Polarimetry using liquid-crystal variable retarders: theory and calibration", J. of Optics A: Pure and Applied Optics **2**, 216-222 (2000)
5. L. J. November, L. M. Wilkins, "Liquid Crystal polarimeter: a solid state imager for solar vector magnetic fields", Opt. Eng. **34**, 16591668 (1995)
6. K. Shinoda, K. Ichimoto, T. Fukuda, J. Shin, "A universal polarimeter using Liquid Crystal variable retarders at the Norikura Solar Observatory", Report of the National Astronomical Observatory of Japan **5**, 97-106 (2001)
7. A. Hofmann, "Liquid-crystal-based Stokes polarimeter" in *Polarization Analysis, Measurement, and Remote Sensing III, D.B. Chenault, M. J. Duggin, W. G. Egan, D. H. Goldstein, eds.,* Proc. SPIE **4133**, 44-54 (2000)
8. V. Martinez Pillet, M. Collados, J. Sanches Almeida, V. Gonzalez, A. Cruz-Lopez, A. Manescau, E. Joven, E. Paes, J. J. Diaz, O. Feeney, V. Sanchez, G. B. Scharmer, and D. Soltau. "LPSP & TIP: Full stokes polarimeters for the Canary islands observatories", *Proceedings of High Resolution Solar Physics: Theory, Observations and Techniques*, T.

Rimmele, R. R. Radick, and K. S. Balasubramaniam, Ed., (ASP Conf. Series, Sacramento Peak Summer Workshop, vol. **183** (1999) pp. 264-272.

9. V. Martínez Pillet, J.A. Bonet, M. Collados, L. Jochum, S. Mathew, J. L. Medina Trujillo, B. Ruiz Cobo, J. C. del Toro Iniesta, A. C. López Jiménez, J. Castillo Lorenzo, M. Herranz, J. M. Jerónimo, P. Mellado, R. Morales, J. Rodríguez, A. Álvarez-Herrero, T. Belenguer, R. L. Heredero, M. Menéndez, G. Ramos, M. Reina, C. Pastor, A. Sánchez, J. Villanueva, V. Domingo, J. L. Gasent, and P. Rodríguez, "The Imaging Magnetograph eXperiment for the SUNRISE balloon Antarctica project", in *Optical, Infrared, and Millimeter Space Telescopes*, J. C. Mather, ed., Proc. SPIE **5487**, 1152-1164 (2004).
10. Gonsalves, R.A. and Chidlaw, R., "Wavefront sensing by phase retrieval" in Proceedings of the Society of Photo-Optical Instrumentation Engineers, Applications of Digital Image Processing. III **207**, Tescher A.G., ed. (San Diego, CA, 1979), pp. 27-29
11. A. Graham, G. Kopp, C. Vargas-Aburto and R. Uribe, "Preliminary space environment tests of nematic Liquid Crystals" in *Photonics for Space Environments IV*, Edward W. Taylor; Ed., Proc. SPIE **2811**, 46-50 (1996).
12. F. Berghmans, M. Decréton, K. Zdrodowski, T. Nasilowski, H. Thienpont, I. Veretennicoff, "Radiation effects on nematic Liquid Crystal devices", in *Photonics for Space Environments IV,* Edward W. Taylor; Ed., Proc. SPIE **2811**, 2-11 (1996)
13. P. G. de Gennes, and J. Prost, *The Physics of Liquid Crystals* (Clarendon Press, Oxford, 1993)
14. R. M. A. Azzam, and N. M. Bashara, "Theory and analysis of measurements in ellipsometer systems" in Ellipsometry and Polarized Light" (North Holland Publishing Company, Amsterdam, 1977), pp. 169-173.

15. P. Yeh and, C. Gu, *Optics of Liquid Crystal Displays* (John Wiley & Sons, New York, 1999)

16. S. T. Wu and, D. K. Yang, *Reflective Liquid Crystal Displays* (Wiley, New York, 2001)

17. I. Haller, Thermodynamic and static properties of liquid crystals, Prog. Solid State Chem. **10**, 103-112 (1975).

18. I. Chirtoc, M. Chirtoc, C. Glorieux and J. Thoen, "Determination of the order parameter an its critical exponent for n_{CB} (n=5-8) liquid crystals from refractive index data", Liq. Cryst. **31**, 229-204 (2004).

19. S. R. Restaino, "On the use of liquid crystals for adaptive optics" in *Optical Applications of Liquid Crystals*, L. Vicari, ed. (Institute of Physics Publishing, London, 2003) pp. 118-147.

20. C. A. Nicoletta and A. G. Eubanks "Effect of simulated space radiation on selected optical materials", Appl. Optics **11**, 1365-1370 (1972).

21. "Space Product Assurance: thermal vacuum outgassing test for the screening of space materials", ECSS SECRETARIAT, ESA ECSS-Q-70-02A (1999)

Table 1: General environmental test conditions

Test	Environmental Conditions
Vacuum	• $P = 10^{-6}$ mbar • T= 20 ºC (constant)
Thermal-Vacuum	• **Operational levels:** T= -20 ºC to +40 ºC ($P = 10^{-6}$ mbar) • **Non-Operational levels:** T= -65 to 70 ºC ($P = 10^{-6}$ mbar)
Vibration/ dynamic test	• **Random vibration:** Time: 120 s. Flat profile at 0.5 g^2/Hz between 20 and 800 Hz. Decrease 0.5 g^2/Hz at 800 Hz until 0.01g^2/Hz at 2000 Hz $T = 22 \pm 5$ °C, RH= 50% ± 10% and P = 1 atm • **Shock loads** of 10 g (11 ms half sine shock pulse) to analyze ultimate structural failure $T = 22 \pm 5$ °C, RH= 50% ± 10% and P = 1 atm
Outgassing	• $P < 10^{-3}$ Pa; T = 125 ºC, Δt = 24 hour
Gamma Radiation	• 10, 20 and 54 krad at 0.5 krad/h
UV Radiation	• ~30, ~ 60, ~150 and ~180 ESH [(1)]

[(1)] ESH: Equivalent Sun Hours= 94.6 W/m^2

Table 2: Outgassing results of each component, where [(1)] WLT: Weight Loss Total, [(2)] WLR: Weight Loss Recover and [(3)] VCM: Volatile Condensable Mass

	[(1)] WLT %	[(2)] WLR %	[(3)] VCM %
Struct Bond XN-5A	4.149	3.240	0.001
ThreeBond 3026 B	3.317	2.440	0.001
ThreeBond 5030	4.421	3.477	0.155
Cables	0.565	0.441	0.140

List of Figure Captions

1. Fig. 1. LCVRs' structure and dimensions.
2. Fig. 2. Setup for retardance, response time and wavefront error measurements inside the TVC
3. Fig. 3. Retardance measurements of one LCVR-V at +20, +33.5, +40, -20 and +20 ºC after having undergone 7 temperature cycles.
4. Fig. 4: Retardance versus absolute temperature including fits of the experimental data with Haller's approximation.
5. Fig. 5. Retardance versus temperature for different V_p applied: 0, 4, 8 and 14 V.
6. Fig. 6. Response times versus temperature for different voltage changes. The lines show the fit of the experimental data. *Case 3* and *Case 4* data have been multiplied by 5 in order to be able to visualize the plot better.
7. Fig. 7. Wavefront error (rms) versus temperature when V_p = 0 V (In λ units: the Fizeau interferometer has a HeNe laser, λ = 633 nm).
8. Fig. 8. Transmittance of two LCVRs before and after the thermal-vacuum test: a) Data of the LCVR after the whole time thermal-vacuum test for retardance-response measurements and 2 months after the finalization of the test (no-voltage was applied to the LCVR); b) Data of the LCVR after the thermal-vacuum test for wavefront error measurements.
9. Fig. 9. Retardance versus peak voltage after irradiation of 10, 20 and 54 krad for complete voltage range.
10. Fig. 10. Transmittance measured after different total doses of γ irradiation. Inset: Transmittance versus Total dose for λ = 525.5 (IMaX working wavelength)
11. Fig. 11. Transmittance versus wavelength and ESH of two LCVRs before and after different exposures to UV irradiation.

12. Fig. 12. Retardance measured during an increasing voltage cycle before and 1 week after the Vibration Test versus V_p

Figure 1

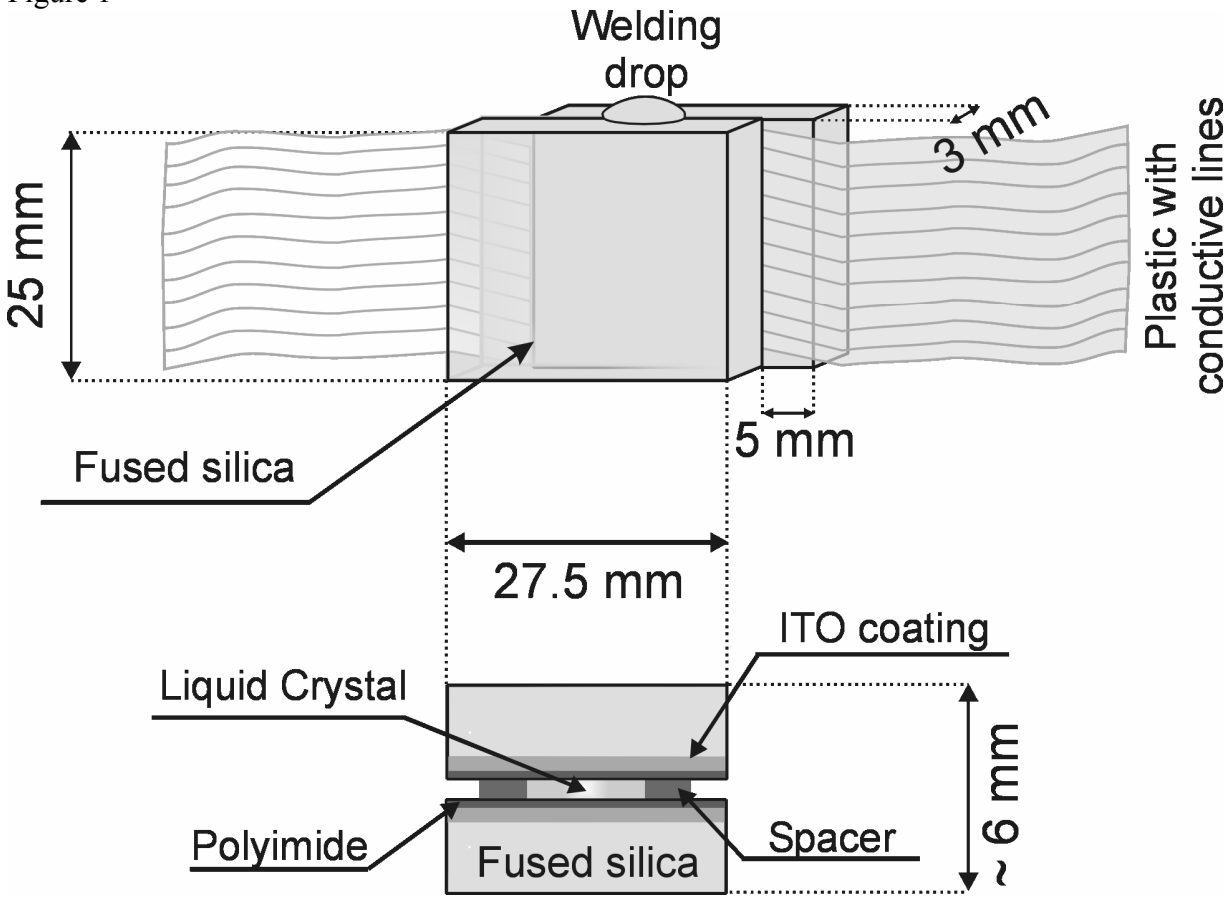

Welding
drop
3 mm
Plastic with
conductive lines
25 mm
Fused silica
5 mm
27.5 mm
ITO coating
Liquid Crystal
6 mm
Polyimide
Fused silica
Spacer

Figure 2

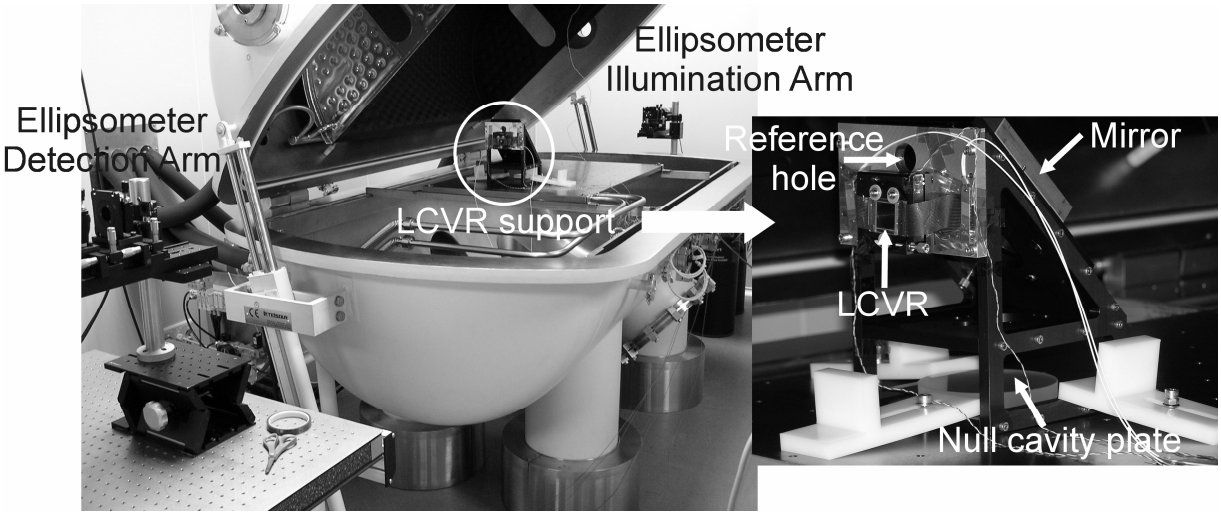

Ellipsometer
Detection Arm
Ellipsometer
Illumination Arm
LCVR support
Reference
hole
Mirror
LCVR
Null cavity plate

Figure 3

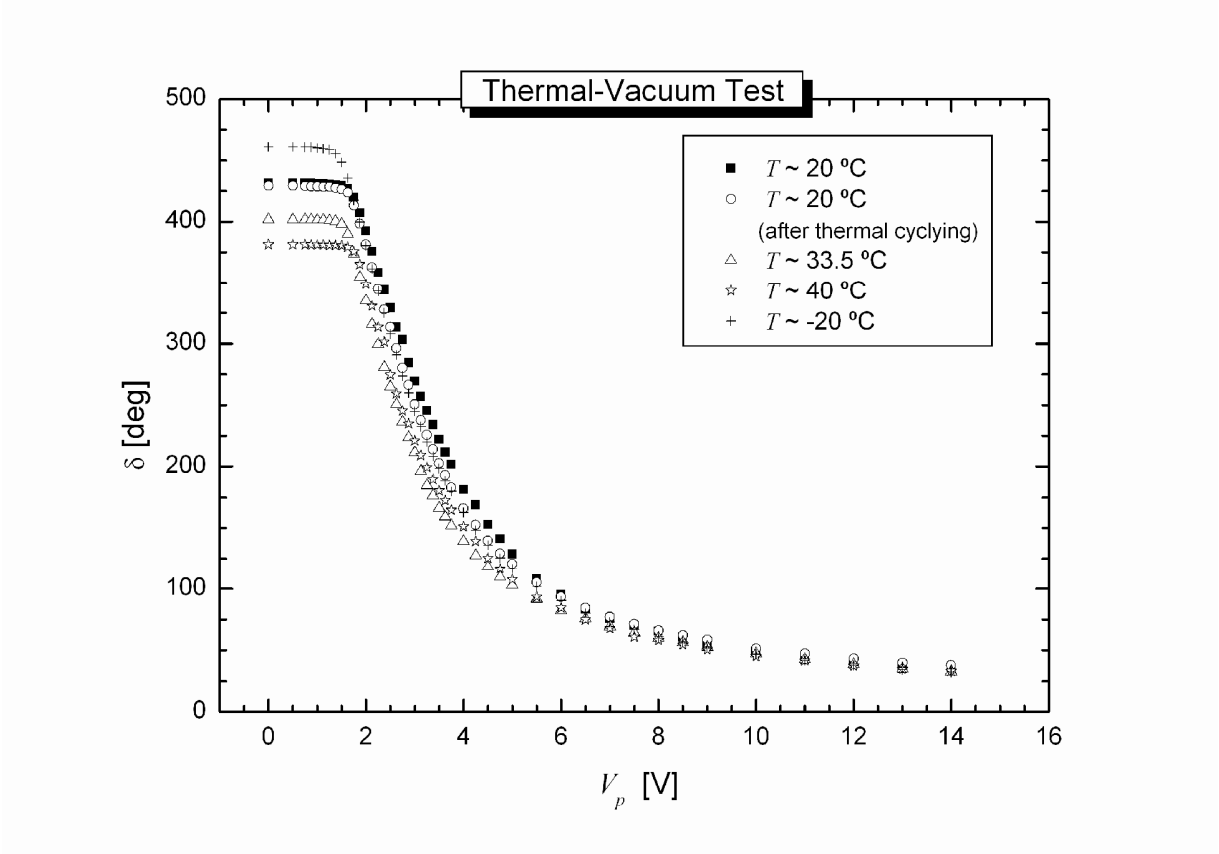

Thermal-Vacuum Test
T ~ 20 ºC
T ~ 20 ºC
(after thermal cyclying)
T ~ 33.5 ºC
T ~ 40 ºC
T ~ -20 ºC
δ [deg]
0
100
200
300
400
500
0
2
4
6
8
10
12
14
16
V_p [V]

Figure 4

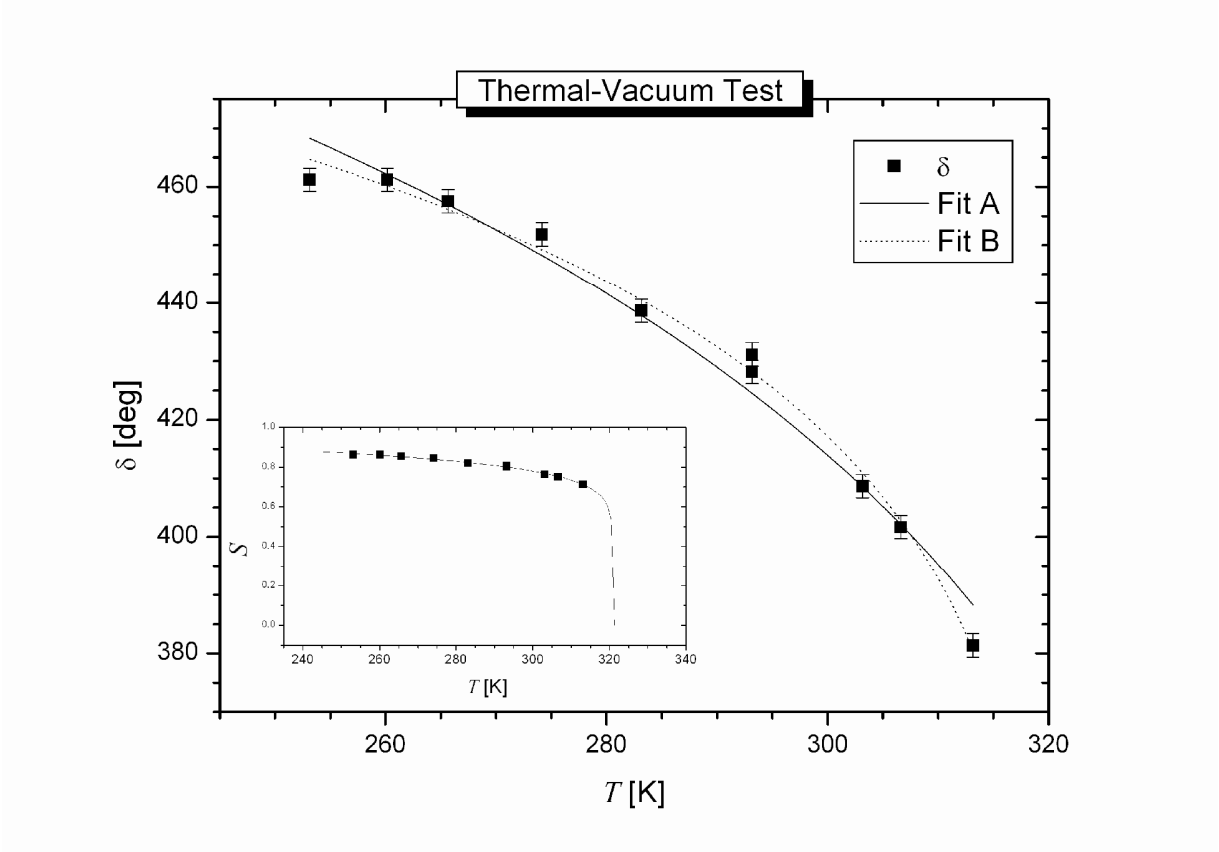


Figure 5

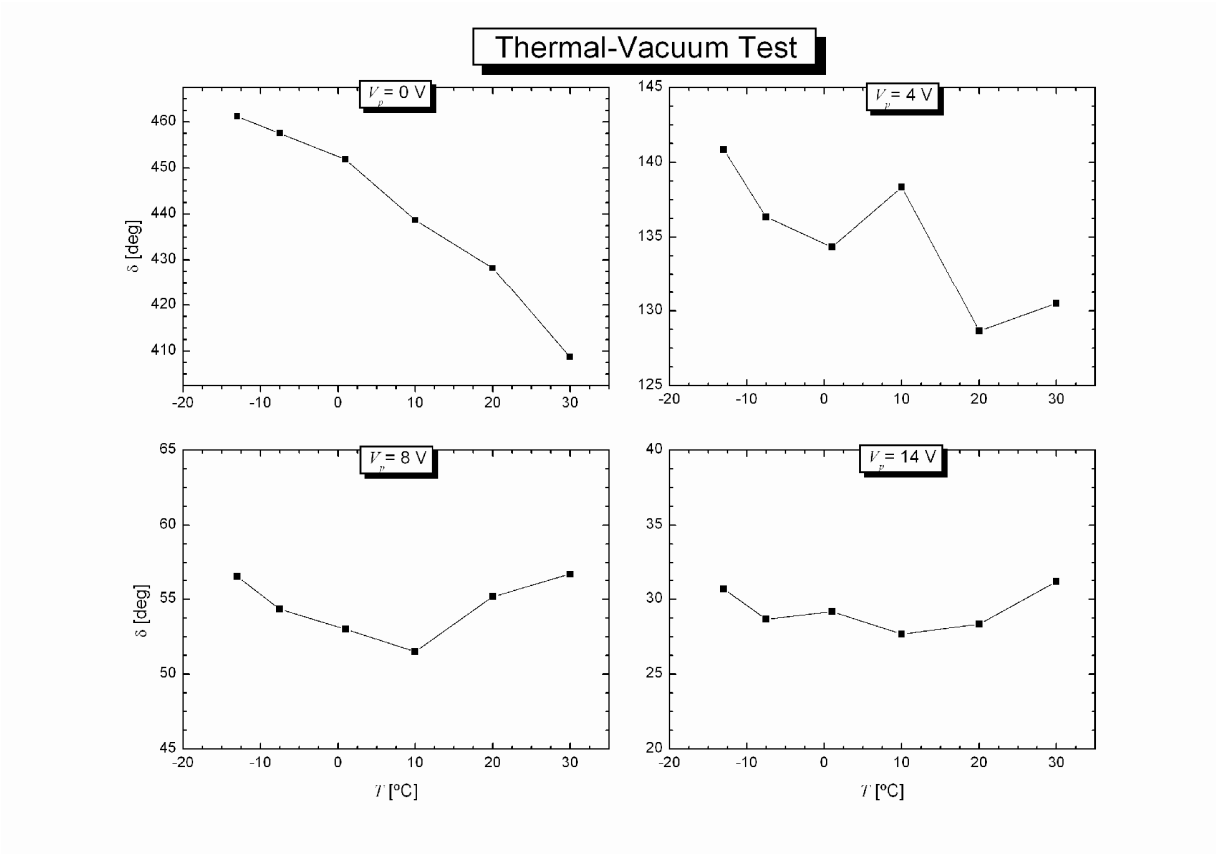


Figure 6

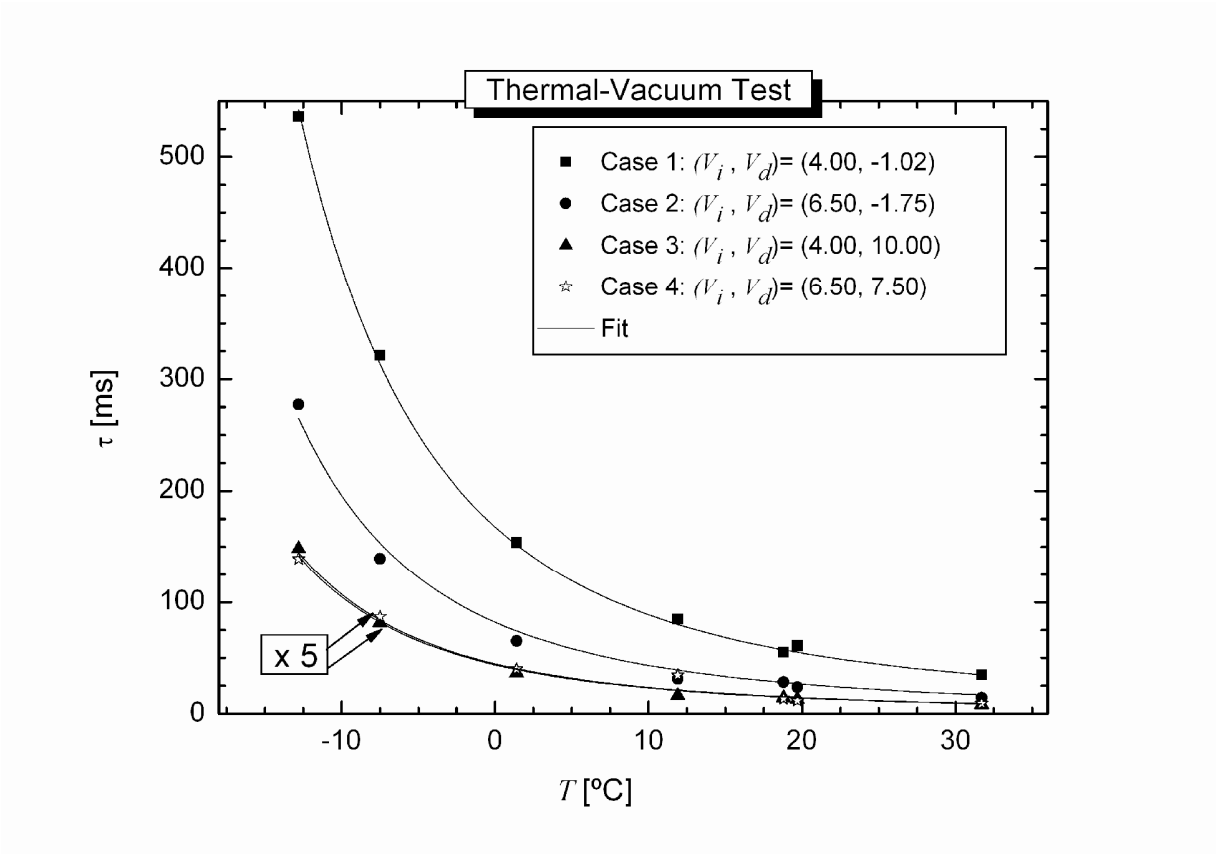

Thermal-Vacuum Test
Case 1: (V_i , V_d)= (4.00, -1.02)
Case 2: (V_i , V_d)= (6.50, -1.75)
Case 3: (V_i , V_d)= (4.00, 10.00)
Case 4: (V_i , V_d)= (6.50, 7.50)
Fit
x 5
τ [ms]
T [ºC]
0
100
200
300
400
500
-10
0
10
20
30

Figure 7

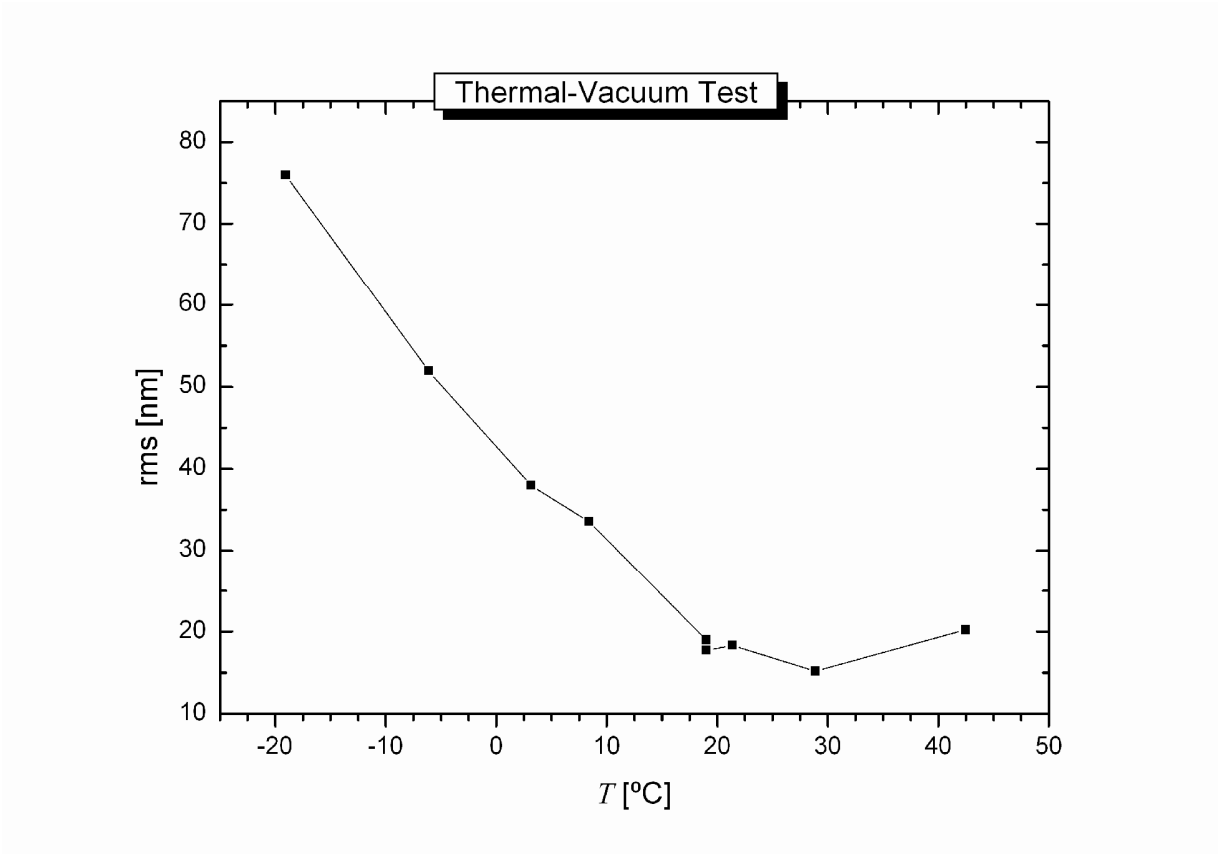
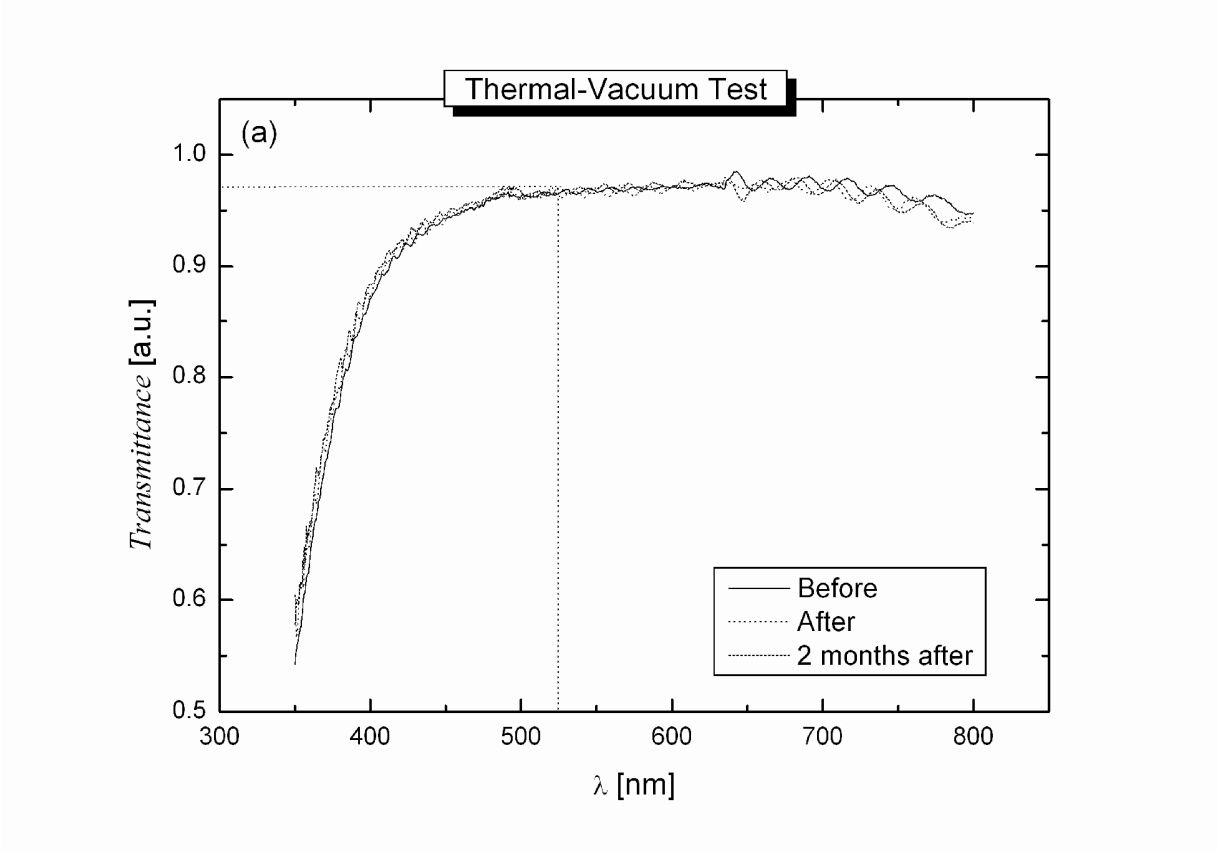

Thermal-Vacuum Test
rms [nm]
80
70
60
50
40
30
20
10
-20
-10
0
10
20
30
40
50
T [ºC]

Figure 8


Thermal-Vacuum Test
(a)
1.0
0.9
0.8
0.7
0.6
0.5
Transmittance [a.u.]
300
400
500
600
700
800
λ [nm]
Before
After
2 months after

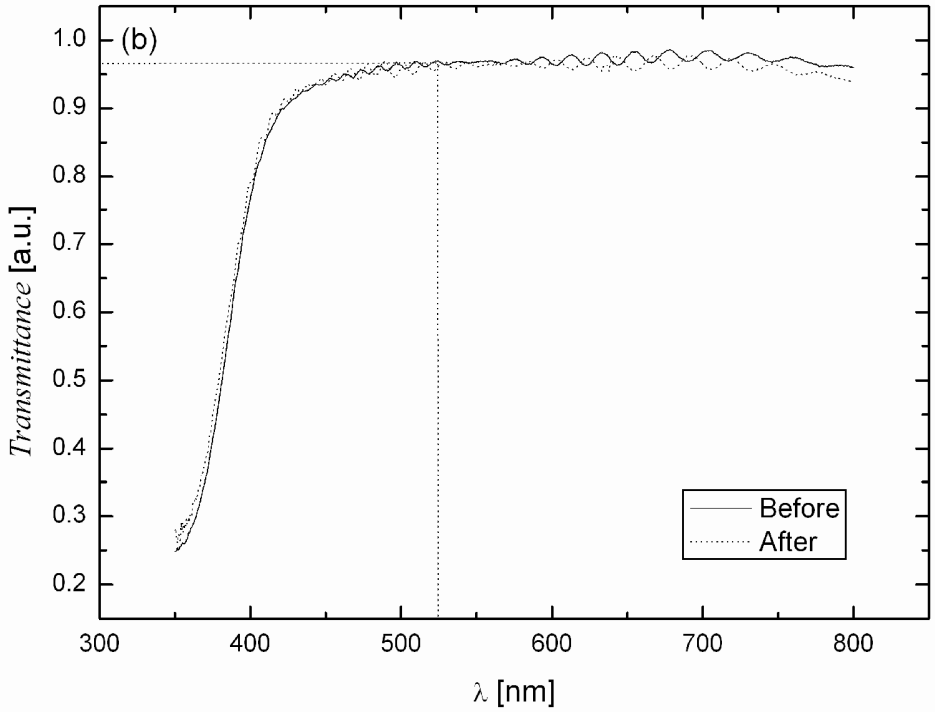

(b)
1.0
0.9
0.8
0.7
0.6
0.5
0.4
0.3
0.2
Transmittance [a.u.]
300
400
500
600
700
800
λ [nm]
Before
After

Figure 9

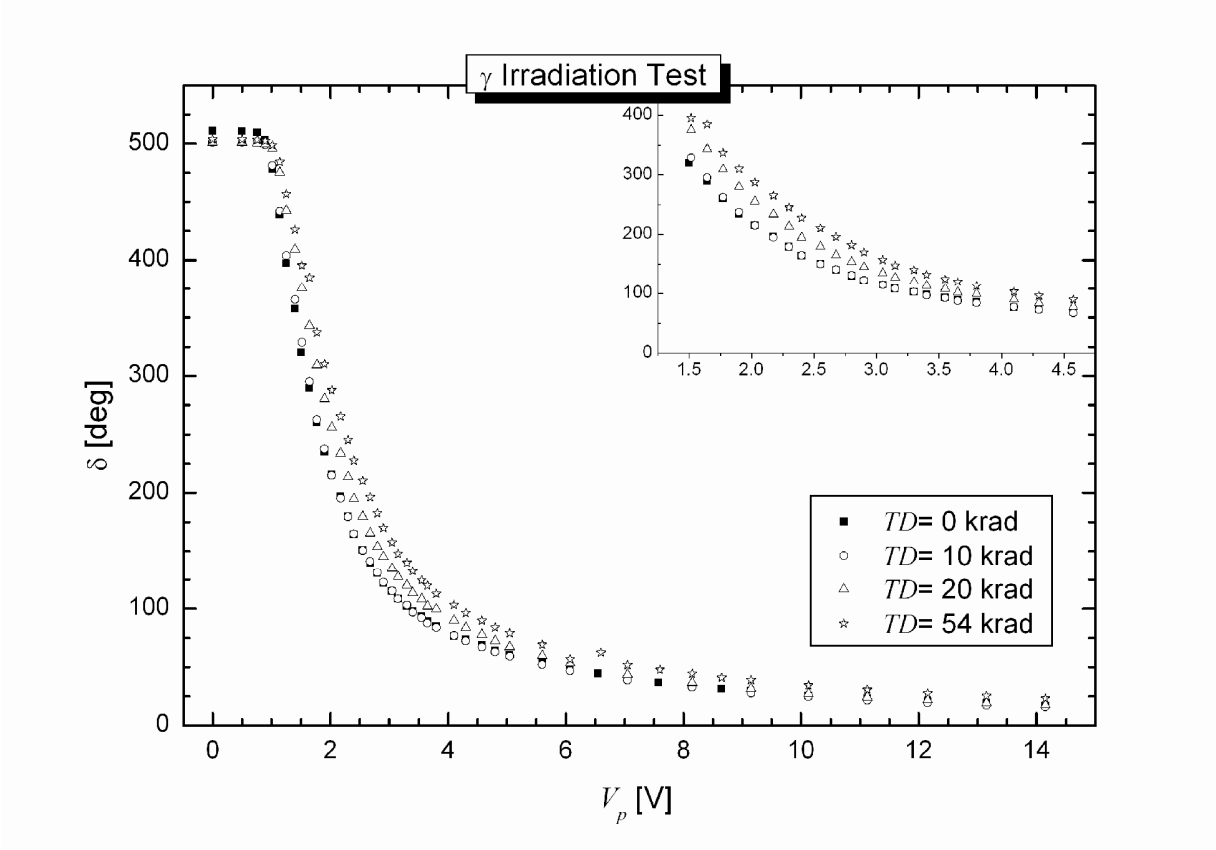

γ Irradiation Test
δ [deg]
V_p [V]
TD= 0 krad
TD= 10 krad
TD= 20 krad
TD= 54 krad

Figure 10

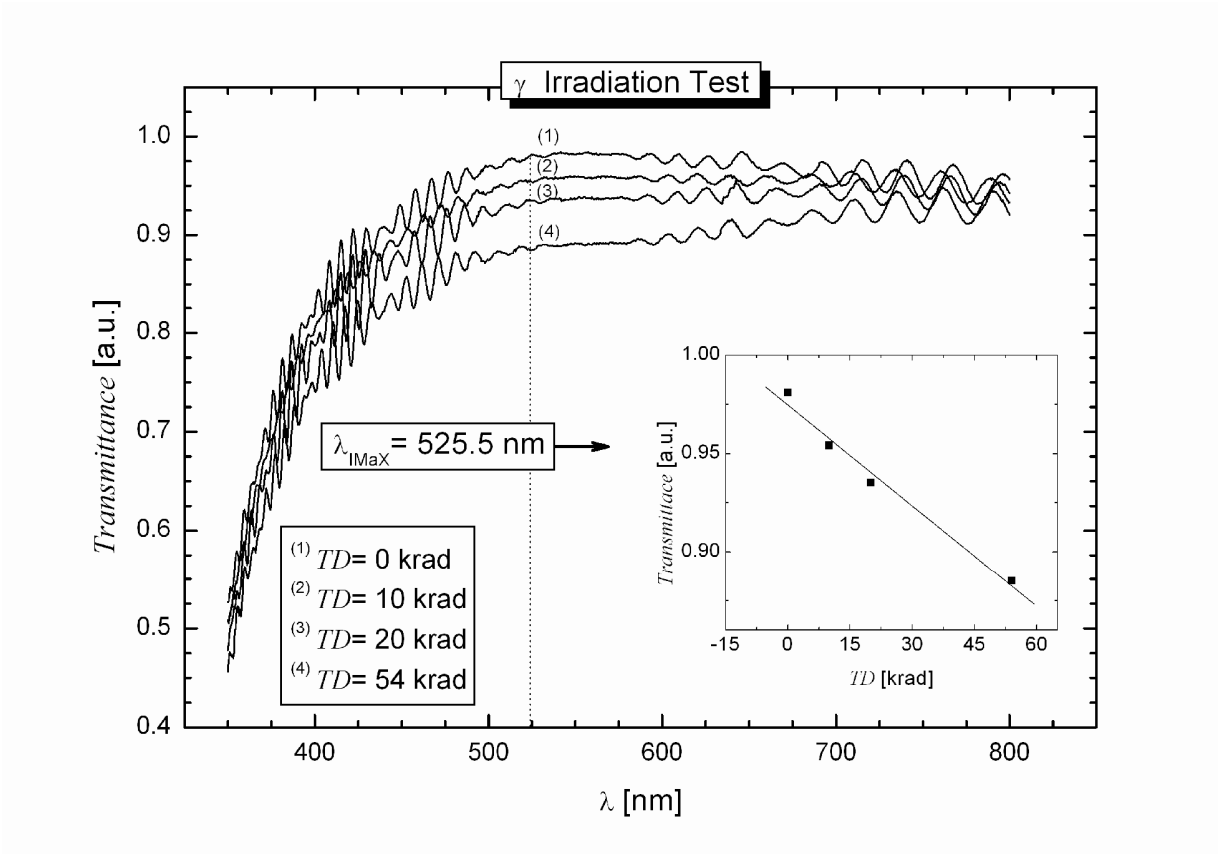
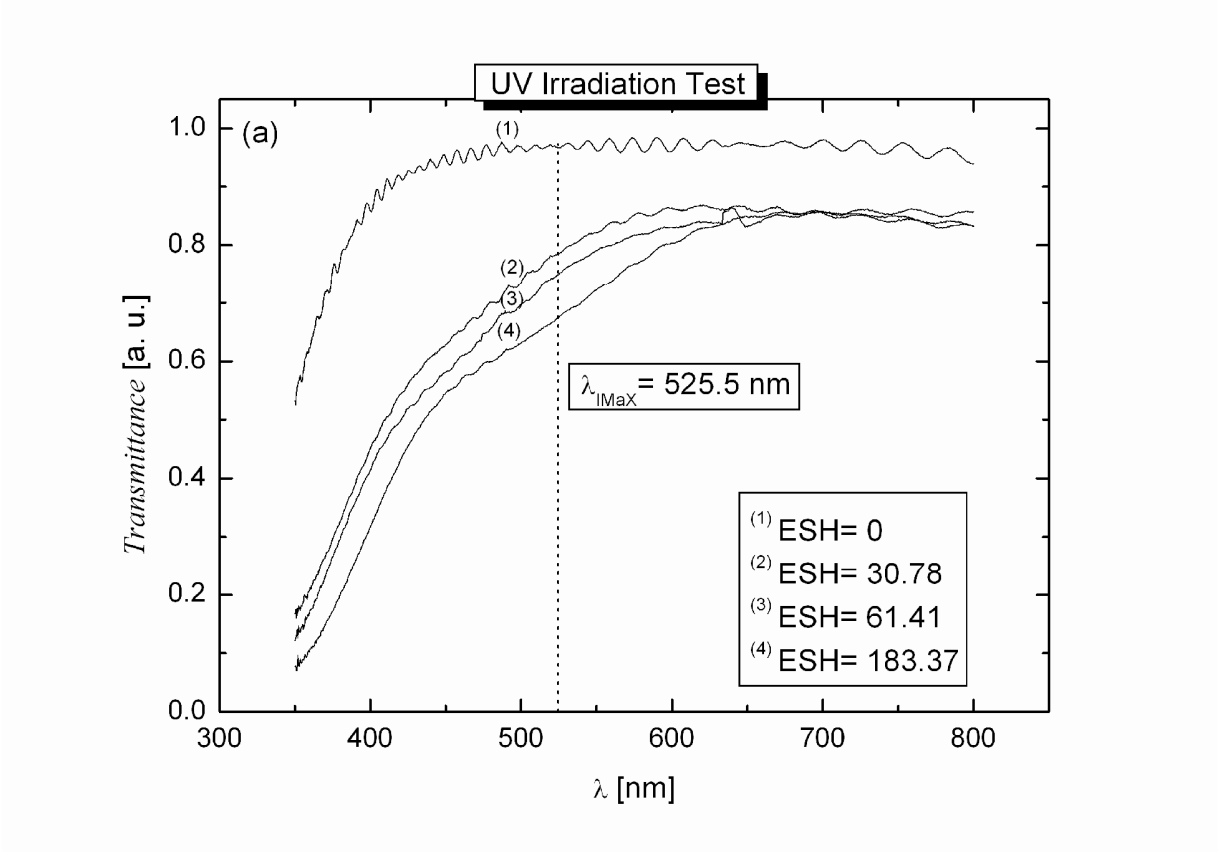

γ Irradiation Test
Transmittance [a.u.]
λ [nm]
(1)
(2)
(3)
(4)
λIMaX= 525.5 nm
(1) TD= 0 krad
(2) TD= 10 krad
(3) TD= 20 krad
(4) TD= 54 krad
Transmittace [a.u.]
TD [krad]

Figure 11


UV Irradiation Test
(a)
(1)
(2)
(3)
(4)
λIMaX= 525.5 nm
(1) ESH= 0
(2) ESH= 30.78
(3) ESH= 61.41
(4) ESH= 183.37
Transmittance [a. u.]
λ [nm]
1.0
0.8
0.6
0.4
0.2
0.0
300
400
500
600
700
800

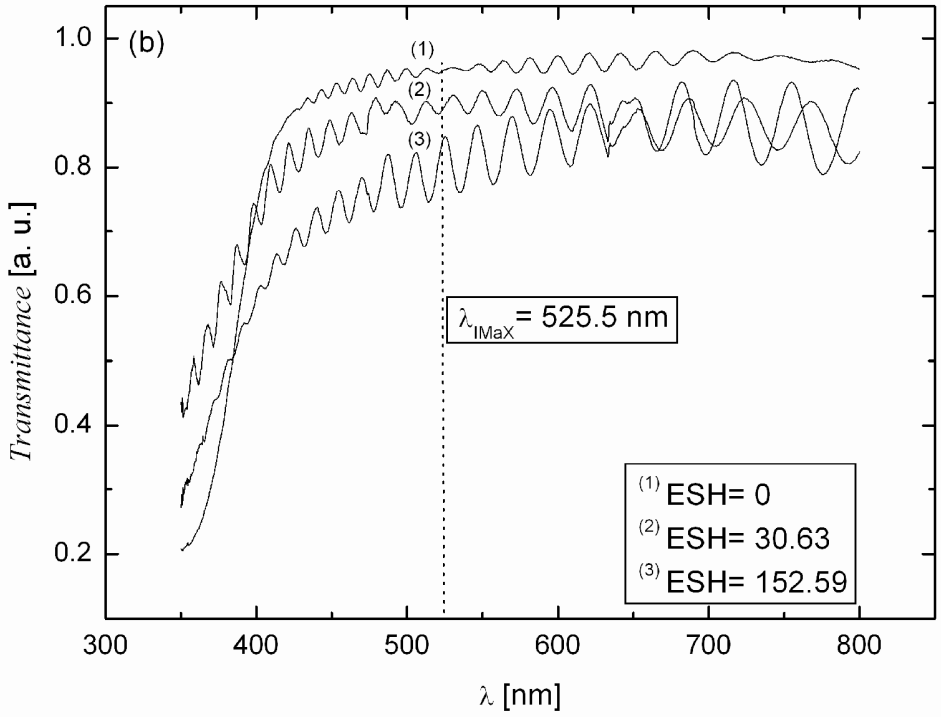

(b)
(1)
(2)
(3)
1.0
0.8
0.6
0.4
0.2
Transmittance [a. u.]
λIMaX= 525.5 nm
(1) ESH= 0
(2) ESH= 30.63
(3) ESH= 152.59
300
400
500
600
700
800
λ [nm]

Figure 12

SE QUITA

